Polarization dynamics across the morphotropic phase boundary in Ba(Zr0.2Ti0.8)O3-x(Ba0.7Ca0.3)TiO3 ferroelectrics

Sergey Zhukov, Yuri A. Genenko, Matias Acosta, Heide Humburg, Wook Jo, Jürgen Rödel, and Heinz von Seggern

Citation: Applied Physics Letters **103**, 152904 (2013); doi: 10.1063/1.4824730

View online: http://dx.doi.org/10.1063/1.4824730

View Table of Contents: http://scitation.aip.org/content/aip/journal/apl/103/15?ver=pdfcov

Published by the AIP Publishing

Polarization dynamics across the morphotropic phase boundary in $Ba(Zr_{0.2}Ti_{0.8})O_3$-$x(Ba_{0.7}Ca_{0.3})TiO_3$ ferroelectrics

Sergey Zhukov,[a] Yuri A. Genenko, Matias Acosta, Heide Humburg, Wook Jo, Jürgen Rödel, and Heinz von Seggern
Institut für Materialwissenschaft, Technische Universität Darmstadt, Petersenstrasse 23, 64287 Darmstadt, Germany

(Received 8 July 2013; accepted 25 September 2013; published online 8 October 2013)

Analysis of polarization switching dynamics by means of the inhomogeneous field mechanism model allows insight into the microscopic mechanism of reversed polarization domain nucleation. For all chemical compositions studied, two distinct field regions of nucleation are established. In the high-field region, the activation energy barrier is found to be inversely proportional to the local field according to the Merz law. In contrast, the barriers in the low-field region exhibit a linear field dependence with a minimum in the compositional region of phase instability, which can explain the corresponding peak ferroelectric properties. © *2013 AIP Publishing LLC*. [http://dx.doi.org/10.1063/1.4824730]

Dynamic properties of polarization switching in polycrystalline ferroelectrics play an important role in microelectronic applications, such as ferroelectric memories[1] and micromechanical applications, such as piezoelectric sensors and actuators.[2] Furthermore, they give insight in micro- to mesoscopic mechanisms of switching allowing optimization of ferroelectric properties by compositional and structural tuning. Of particular interest is the variation of dynamic characteristics and underlying microscopic parameters across the regions of phase transitions where they often experience substantial changes. The problem of analysis is that polycrystalline ferroelectrics typically exhibit a complicated dispersive switching response which cannot be interpreted in terms of the classical nucleation and growth theory often referred to as the Kolmogorov-Avrami-Ishibashi (KAI) model.[3] To obtain microscopic parameters providing the macroscopic switching process, more sophisticated theories are required, which account for a statistical distribution of local switching times in a system.[4–8] To this end, the inhomogeneous field mechanism (IFM) model is used in this paper, which derives the distribution of times from the distribution of randomly distributed local field values.[7,8] The lead-free $(1-x)Ba(Zr_{0.2}Ti_{0.8})O_3$-$x(Ba_{0.7}Ca_{0.3})TiO_3$ ferroelectrics (referred to as BCZT100x hereafter) were chosen for this case study for their prominent properties, which are discussed in the following.

In 2009, Liu and Ren[9] first reported on BCZT100x ceramics that showed piezoelectric coefficients, d_{33}, of 560–620 pm/V for $x = 0.5$ (BCZT50) at room temperature, which clearly exceed the values of competing lead-free materials based on bismuth sodium titanate (BNT)[10] and even those of most lead zirconate titanate (PZT)[10,11] materials. In addition, it exhibits high electromechanical coupling factors of 0.46–0.65 (Refs. 12 and 13) and a low coercive field strength E_C of about 0.2 kV/mm.[9,12] A large-signal piezoelectric coefficient, d_{33}*, as large as 1150 pC/N at 0.5 kV/mm has been reported, albeit only in a small temperature range .[9,12] A remanent polarization of 14.5 μC/cm^2 and a very high dielectric permittivity $\varepsilon \sim 3000$,[9] which is comparable to that of soft PZT materials (2000–3500) (Refs. 10 and 11) and different lead-free piezoelectrics (200–3300),[10] complete the set of interesting properties of BCZT50.

Liu and Ren also proposed that BCZT100x solid solutions possess a morphotropic phase boundary (MPB), where piezoelectric properties peak.[9] At room temperature, this boundary is at $x \sim 0.5$ between a rhombohedral (R) and a tetragonal (T) phase, although the exact phase diagram in BCZT100x is still controversial.[9,12–18] For example, a recent study[18] suggested that an intermediate orthorhombic (O) phase and a phase convergence region where four phases (R, O, T, and cubic (C)) may occur in a narrow temperature and compositional range. Thereby, the existence of such polymorphic regions seems to be a key to achieving the outstanding piezoelectric performance. It is generally believed that the composition-induced ferroelectric-ferroelectric transition causes an instability of the polarization state with very low energy barriers for polarization rotation between co-existing phases or even vanishing polarization anisotropy.[19–21] As expected, the mobility of the domain walls near the MPB may be considerably enhanced, thus influencing the polarization switching process.

The main objective of the current research is to investigate the variation of the polarization kinetics for BCZT100x ceramics with compositional changes in x providing a transition across the morphotropic phase boundary at room temperature. The activation parameters of the switching kinetics throughout the morphotropic phase boundary are not available despite their salient insight into the nature of the instability. To this end, six compositions with $x = 0.35$, 0.45, 0.48, 0.50, 0.52, and 0.60 were synthesized, and the polarization switching has been studied over broad time and field domains covering the ranges from 1 μs to 10^3 s and 0.01 kV/mm to 1.5 kV/mm, respectively. From earlier structural investigations mentioned above, it can be implied that at room temperature, BCZT35 and BCZT60 consist of single R and T phases, respectively. On the other hand, the other compositions are not assigned and, therefore, belong to the instability region between rhombohedral, tetragonal, and, presumably, orthorhombic phases.

[a]Author to whom correspondence should be addressed. electronic mail: zhukov@e-mat.tu-darmstadt.de

The BCZT100x powders were synthesized by a mixed solid state route using oxides and carbonates (Alfa Aesar GmbH & Co. KG). The raw chemicals $BaCO_3$, TiO_2, $CaCO_3$, and ZrO_2 with purities above 99.5% were mixed according to the stoichiometric formula. All the powders were ball-milled in home-made nylon containers in a planetary ball mill (Fritsch Pulverisette 5) for 5 h at 250 rpm utilizing yttria stabilized zirconia balls and ethanol and subsequently dried at 90 °C. The powders were calcined at 1300 °C for 2 h and ball-milled again for 15 h with the same parameters as previously used. Disc-shape samples of 10 mm in diameter and 0.5 to 0.7 mm in thickness were cold-isostatically pressed (KIP 100 E, Weber-Pressen) at 300 MPa. The green bodies were sintered in covered zirconia crucibles under atmospheric pressure at 1500 °C for 2 h. Sintered pellets were ground, polished, and silver paste electrodes were applied on both sides. The electrodes were burnt-in at 400 °C for 2 h before electrical characterization was performed.

A pulse switching method was utilized to measure the reversed polarization ΔP as a function of time for an applied electric field E_m.[22] Therefore, the samples were fully poled in one direction for a long time and the switching was performed utilizing an oppositely biased voltage pulse. The pulse duration ranged from 1 μs to 10^3 s. The sample thereby was in series with a current limiting resistor of $R = 133\ \Omega$ and a measuring capacitor $C_m = 4.4\ \mu$F, much larger than the sample capacitance. The temporal evolution of the electric displacement was detected by the measuring capacitor C_m and recorded by means of a digital oscilloscope. The time constant of the utilized electrical circuit was calculated to be about 200 ns, taking the ferroelectric polarization into account. Thereby, the time constant was shorter than the shortest voltage pulse applied during the experiments. More details about the measurement setup can be found elsewhere.[22]

The experimental procedure was designed to focus solely on the switching contribution to polarization. The temporal response of the reversed polarization ΔP at an applied electric field E_m is determined in four steps: (1) the sample is poled by a negative DC field of 1 kV/mm ($\sim 5E_C$) for 300 s followed by short circuiting for 60 s assuring that the saturation polarization $-P_S$ is reached after such a procedure. (2) A positively directed switching field E_m is applied to the sample for a certain time t followed again by short circuiting, and the electric displacement is recorded by a digital oscilloscope (Tektronix TDS 3014). (3) The sample is poled again for 300 s but this time by a positive DC field of 1 kV/mm to achieve its saturated $+P_S$ state. (4) Finally, forward poling on the fully poled sample is performed by applying the positive field E_m to the sample for a time period t for the second time. The recorded apparent displacement during forward poling contains all those components which exist in the switching experiment (step two) except for the switched ferroelectric polarization ΔP. Therefore, the net switched polarization $\Delta P(E_m, t)$ is calculated as the difference between the electric displacement values of switching and forward poling taken at time t after application of the electric field E_m. We note that the switching characteristics as well as the P-E loops have not changed in the course of measurements.

Using the above procedure, the polarization ΔP has been measured for 25 different external electric fields E_m all applied over a long observation time. Thereby, one obtains ΔP as a function of time t and field E_m, thus establishing a matrix $\Delta P(E_m, t)$ for all compositions investigated. Figure 1 displays the temporal development of ΔP for three selected compositions: (a) BCZT50, (b) BCZT35, and (c) BCZT60 representing the MPB region, R phase, and T phase, respectively.

Traditionally, the polarization switching kinetics is described by the KAI model,[3] which suggests a temporal dependence of the reversed polarization as follows:

$$P(t,\tau) = \Delta P_{\max}\left\{1 - \exp\left[-\left(\frac{t}{\tau}\right)^{\beta}\right]\right\}, \qquad (1)$$

where t is the time elapsed after application of the step field E_m, ΔP_{max} is the amount of the reversed polarization reached at saturation, while τ is the characteristic switching time, and β the so-called Avrami exponent. The β parameter depends on the dimensionality of the domain nucleus and is expected to adopt only integer values from 1 to 3.

It should be noted that the experimental results depicted in Fig. 1 cannot be fitted satisfactorily by the KAI model. Therefore, the recently introduced IFM model[7,8] was utilized to analyze the switching properties of BCZT100x ceramics.

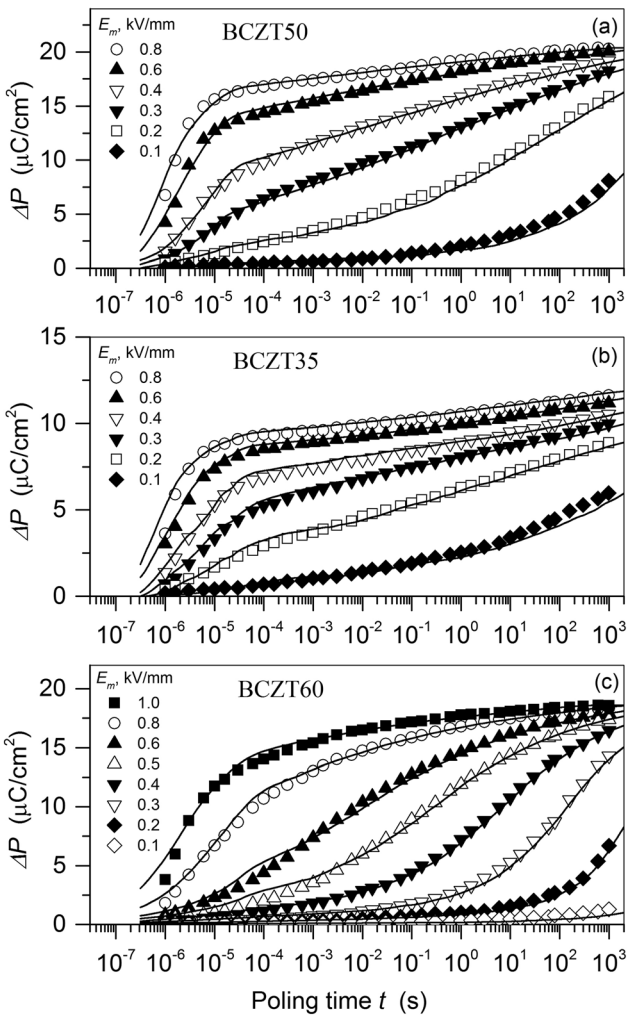

FIG. 1. Switched polarization ΔP versus poling time for BCZT50 (a), BCZT35 (b), and BCZT60 (c). Symbols correspond to the experimental results measured at different fields E_m as indicated. Solid curves represent the field-related IFM model calculations by the Eq. (2).

This model assumes a statistical distribution of switching times due to a distribution of local field values. It has been shown that the IFM model describes reliably the polarization reversal in different classes of ferroics including examples with rather complex switching behavior such as fatigued PZT ceramics[7] and ferroelectric polymers.[23] In fact, the switching response in BCZT100x is also rather multifarious. This is particularly seen for BCZT50 in Fig. 1(a), where the initial fast rise at times shorter than about 3×10^{-5} s is followed by a slow increase with nearly linear dependence on logarithmic time scale. As a result, a very long time up to 100 s is required to complete the switching process even when a high field of $E_m = 0.8$ kV/mm ($\sim 4E_C$) is applied to the sample. Moreover, the amount of polarization switched during the fast step drastically decreases with lowering the switching field E_m. Similar features were captured for all compositions investigated.

In the context of the IFM model, the switching response is expressed as

$$\Delta P(E_{\mathrm{m}}, t) = \Delta P_{\max} \int_0^{E_{\mathrm{m}}/E_{\max}(t)} \frac{du}{u}\, \Phi(u), \qquad (2)$$

where $\Phi(E_m/E_{max}(t))$ is the scaled normalized logarithmic derivative $1/\Delta P_{max} \times \partial \Delta P/\partial(ln\ E_m)$ and $E_{max}(t)$ is the maximum position of this derivative as a function of field established for different observation times.

In the following, it will be demonstrated how two functions $\Phi(\mathrm{E_m}/\mathrm{E_{max}}(\mathrm{t}))$ and $E_{max}(t)$ are obtained from the experiment. First, the field development of ΔP for fixed observation times t is plotted, as demonstrated in Fig. 2(a) for BCZT50. Then, the logarithmic derivatives are calculated and normalized by ΔP_{max} of 20.8 μC/cm^2 obtained from Fig. 2(a). Resulting curves for different observation times are plotted in Fig. 2(b). It is seen that the amplitudes of the maxima are practically independent of the actual value of the observation time. The scaling of E_m values of each curve in Fig. 2(b) to its own maximum value E_{max} leads to a master curve $\Phi(E_m/E_{max}(t))$ (Fig. 2(c)), which is a precondition of the applicability of the IFM model. This master curve is virtually independent of the observation time and can be considered as a fingerprint of the system, which contains information about the statistical field distribution. The latter distribution can be restored from Φ as was demonstrated elsewhere.[7,8]

Fig. 3 displays the experimentally determined E_{max} values for different observation times t for the BCZT50 ceramic. $E_{max}(t)$ thereby reflects the actual field dependence of the local switching times $\tau(E)$, where E represents the local electric field. Different empirical and theoretical expressions for $\tau(E)$ have been proposed to relate the switching time to the applied electric field.[24–28] At this point, it should be noted that the IFM model does allow a free choice of the mechanism for the reverse domain nucleation and growth, and does not assume *a priori* a certain microscopic switching scenario. The experimental function $E_{\max}(t)$ can, however, help to select the suitable theoretical mechanism. This is done by solving the equation $E_{\max}(t)/\gamma = E$ with respect to t, thus obtaining the field dependence of the local switching time $\tau(E)$.[7,8] The parameter γ is calculated from

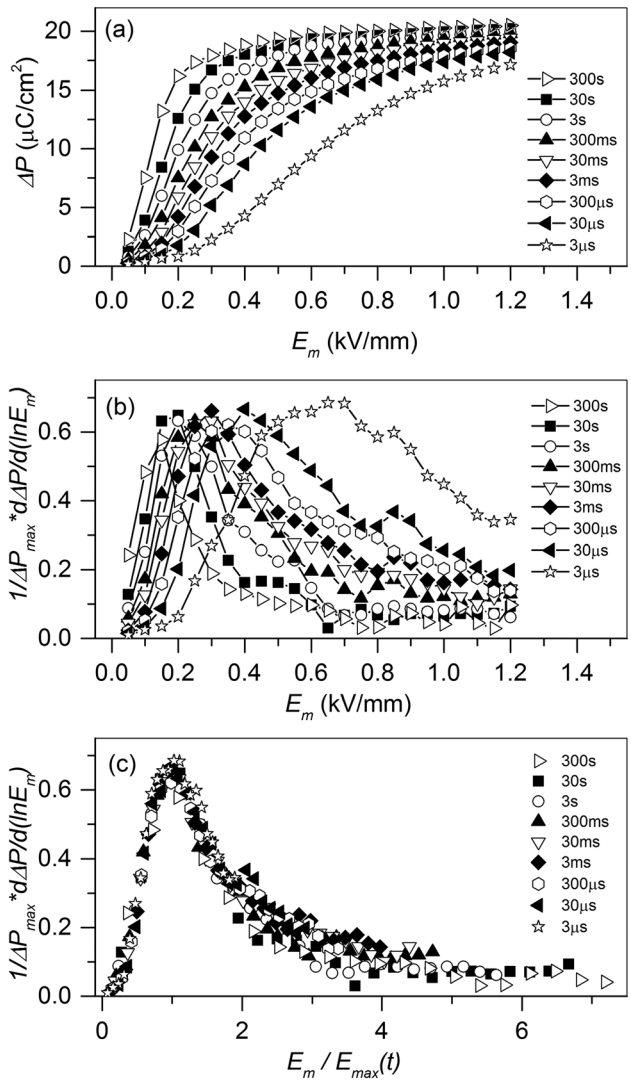

FIG. 2. Switched polarization ΔP of BCZT50 versus applied field E_{m} at different observation times t as indicated (a), its normalized logarithmic derivatives versus applied field (b), and the same derivatives scaled to their maximum positions $E_{\max}(t)$ (c).

the shape of the master curve Φ and typically assumes values around unity.[7,8]

For BCZT50, the function $E_{\max}(t)$ exhibits two distinct time dependences with electric field: (I) $E < 0.4$ kV/mm and (II) $E > 0.4$ kV/mm as marked in Fig. 3. For higher fields, the dependence $E_{\max}(t) = E_{\mathrm{a}} / [\ln(t/\tau_0)]$ applies, which

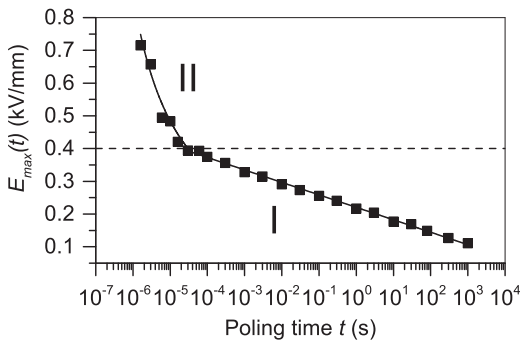

FIG. 3. $E_{max}(t)$ versus observation times t for BCZT50. Symbols correspond to the experimental data, whereas the solid lines represent the fits by the functions $E_{\max}(t) = \mathrm{A} - \mathrm{B} \times \ln(t/\tau_0)$ (I) and $E_{\max}(t) = \mathrm{E_a}/\ln(t/\tau_0)$ (II). The utilized fitting parameters are shown in Table I.

corresponds to either Merz law[24] $\tau = \tau_0 \times \exp(E_a/\gamma E)$ or its advanced form for domain wall creep motion.[25] For lower fields, the dependence becomes virtually linear on the logarithmic time scale and can be well fitted by the function

$$E_{\max}(t) = A - B \times \ln\left[\frac{t}{\tau_0}\right], \tag{3}$$

with A and B being constants. This behaviour corresponds to the field dependence

$$\tau(E) = \tau_0 \times \exp\left[\frac{A - \gamma E}{B}\right]. \tag{4}$$

Such a linear field dependence of the activation energy and the corresponding logarithmic time dependence of the characteristic fields have been reported for small electric fields and were related to microscopic parameters utilizing the non-equilibrium polarization-switching model by Vopsaroiu *et al.*[27,28] They used

$$A = \frac{\gamma W_B}{P_S} \text{ and } B = \frac{\gamma k_B T}{P_S V^*}, \tag{5}$$

where k_B is the Boltzmann constant, T absolute temperature, W_B the thermodynamic activation barrier per unit volume at zero applied electric field, and V^* the critical volume of the nucleating domain with reversed polarization. Adopting this theory, the energy of the nucleated domain $W_B^* = W_B \times V^*$ and its dipole moment $P_s \times V^*$ can be evaluated from the experimental data.

The above determined functions $\Phi(E_m/E_{max}(t))$ and $E_{max}(t)$ were used to calculate the temporal polarization switching response by Eq. (2). The results for different applied field strength are displayed in Fig. 1 by solid lines for three selected compositions. In all cases, a good agreement between the experimental data and the IFM model calculations was achieved. Note that for all compositions investigated, the $E_{max}(t)$ dependence exhibits two distinct regions where different fit functions were applied as exemplarily shown for BCZT50 in Fig. 3. The obtained fitting parameters for the $E_{max}(t)$ functions for all compositions were determined from Eqs. (3) to (5) and listed together with parameters extracted from the experiment in Table I. E_{CR} is thereby a field value separating the low- and high-field regimes.

Utilizing these data, it is possible to relate the fitting parameters presented in Table I to the microscopic characteristics such as W_B, V^*, and W_B^* in the low field switching regime for all different compositions. Obtained results are displayed in Figs. 4(a)–4(c), where the symbols correspond to the experimental results and dashed lines are guides for the eye. It can be seen from Figs. 4(a)–4(c) that all microscopic characteristics change with composition. Namely, W_B is increasing, while V^* is decreasing on increasing BCT content. Simultaneously, the parameter W_B^* determined by the product of W_B and V^* has a minimum at x = 0.48 as shown in Fig. 4(c). This implies that the activation energy for the nucleus with a critical volume V^* required for the polarization reversal is minimal in the compositions near MPB, providing the most favorable conditions for polarization switching. The absolute values of the activation barrier W_B^* of about ~0.75 eV are close to those of soft piezoceramic PZT-5 H at the MPB which were reported to exhibit the activation barrier $W_B^* = 0.7$ eV but one order of magnitude smaller nuclei volume V^* of 3×10^{-25} m^3.[28] Concerning the nuclei size Gao *et al.*[17] reported by transmission electron microscopy that the nucleating domains can hardly be seen in the pure tetragonal and rhombohedral phases of BCZT100x, because in these phases, the critical nuclei rapidly develop to their equilibrium domain size which is in the micrometer range. In the phase transition region near the MPB, they report nanodomain features of 20 nm to 100 nm, which are in agreement with our reported V^* values of about 2 to 3×10^{-24} m^3 at x ~0.5 in Fig. 4(b). The reason is likely that two phases coexist, which are constantly converting into each other maintaining a dynamic equilibrium. In this regime, the switching is eased. The effect of the reduced W_B^* is reflected in the achieved total polarization, which is higher near the MPB, indicating that the reduced barrier allows for the switching of otherwise not switchable polarization.

TABLE I. Fitting and measured parameters for BCZTx compositions at +25 °C.

100x (%)	A (kV/mm)	B (kV/mm)	P_S (μC/cm^2)	γ	E_a (kV/mm)	τ_0 (s)	E_{CR} kV/mm
35	0.363	0.0115	6.0	1.03	1.82	9.6×10^{-8}	0.30
45	0.460	0.0160	10.3	1.06	2.17	8.0×10^{-8}	0.36
48	0.556	0.0197	10.0	1.08	2.06	9.1×10^{-8}	0.40
50	0.490	0.0165	10.4	1.15	2.34	7.5×10^{-8}	0.40
52	0.855	0.0275	9.8	1.16	5.45	6.6×10^{-9}	0.59
60	1.053	0.0297	9.3	1.12	8.07	1.3×10^{-9}	0.72

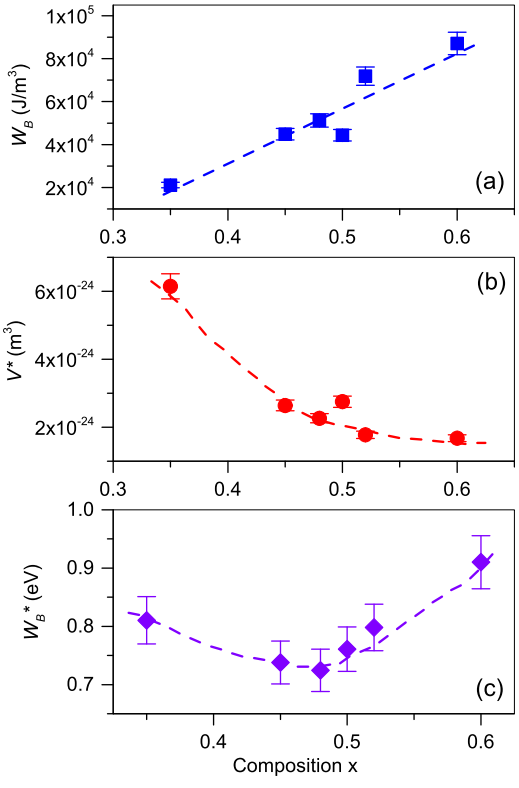

FIG. 4. Thermodynamic activation barrier per unit volume W_B (a), critical volume of the nucleating domain V^* (b), and activation barrier W_B^* (c) for different BCZT100x compositions.

In conclusion, compositional modification was demonstrated to entail substantial variations in the polarization switching behaviour of BCZT100x compounds. The microscopic mechanism underlying the local switching, expressed by the field dependence of the local switching time, cannot be resolved by implementation of the classical KAI model because of the complicated form and dispersive character of the polarization reversal. However, this could be achieved by the application of the IFM model, assuming a statistical distribution of local switching times due to a distribution of local field strengths. The model reveals distinct regimes of polarization reversal in local high- and low-field regions, giving insight into the microscopic mechanisms of polarization switching. For the high-field regions, the switching time appears to follow Merz law in terms of the activation barrier for the nucleation of reversed domains, which is inversely proportional to the local field. For the low-field regions, the barrier depends linearly on the electric field and exhibits a minimum at the morphotropic phase boundary, which is the result of an increasing energy barrier per volume times a decreasing volume of the nuclei with composition x. This rationalizes the peak value of the polarization and the superb electromechanical properties of these compounds at the MPB.

This work was supported by the Deutsche Forschungsgemeinschaft through the Sonderforschungsbereich 595 "Electrical Fatigue in Functional Materials" and the AdRIA Hesse state center for Adaptronics.

[1]J. F. Scott, *Ferroelectric Memories* (Springer, Berlin, 2000).
[2]P. Muralt, J. Micromech. Microeng. **10**, 136 (2000).
[3]H. Orihara, S. Hashimoto, and Y. Ishibashi, J. Phys. Soc. Jpn. **63**, 1031 (1994).
[4]A. K. Tagantsev, I. Stolichnov, N. Setter, J. S. Cross, and M. Tsukada, Phys. Rev. B **66**, 214109 (2002).
[5]J. Y. Jo, H. S. Han, J.-G. Yoon, T. K. Song, S.-H. Kim, and T. W. Noh, Phys. Rev. Lett. **99**, 267602 (2007).
[6]N. Dabra, J. S. Hundal, A. Nautiyal, K. C. Sekhar, and R. Nath, J. Appl. Phys. **108**, 024108 (2010).
[7]S. Zhukov, Y. A. Genenko, O. Hirsch, J. Glaum, T. Granzow, and H. von Seggern, Phys. Rev. B **82**, 014109 (2010).
[8]Y. A. Genenko, S. Zhukov, S. V. Yampolskii, J. Schütrumpf, R. Dittmer, W. Jo, H. Kungl, M. J. Hoffmann, and H. von Seggern, Adv. Funct. Mater. **22**, 2058 (2012).
[9]W. Liu and X. Ren, Phys. Rev. Lett. **103**, 257602 (2009).
[10]J. Rödel, W. Jo, K. Seifert, E. Anton, T. Granzow, and D. Damjanovic, J. Am. Ceram. Soc. **92**, 1153 (2009).
[11]B. Jaffe, W. R. Cook, and H. Jaffe, *Piezoelectric Ceramics* (Academic Press, London, 1971).
[12]D. Xue, Y. Zhou, H. Bao, C. Zhou, J. Gao, and X. Ren, J. Appl. Phys. **109**, 054110 (2011).
[13]F. Benabdallah, A. Simon, H. Khemakhem, C. Elissalde, and M. Maglione, J. Appl. Phys. **109**, 124116 (2011).
[14]M. C. Ehmke, S. N. Ehrlich, J. E. Blendell, and K. J. Bowman, J. Appl. Phys. **111**, 124110 (2012).
[15]D. Damjanovic, A. Biancoli, L. Batooli, A. Vahabzadeh, and J. Trodahl, Appl. Phys. Lett. **100**, 192907 (2012).
[16]H. Bao, C. Zhou, D. Xue, J. Gao, and X. Ren, J. Phys. D: Appl. Phys. **43**, 465401 (2010).
[17]J. Gao, D. Xue, Y. Wang, D. Wang, L. Zhang, H. Wu, S. Guo, H. Bao, C. Zhou, W. Liu, S. Hou, G. Xiao, and X. Ren, Appl. Phys. Lett. **99**, 092901 (2011).
[18]D. S. Keeble, F. Benabdallh, P. A. Thomas, M. Maglione, and J. Kreisel, Appl. Phys. Lett. **102**, 092903 (2013).
[19]D. Damjanovic, Appl. Phys. Lett. **97**, 062906 (2010).
[20]Y. Ishibashi and M. Iwata, Jpn. J. Appl. Phys. Part 2 **37**(8B), L985–L987 (1998).
[21]G. A. Rossetti, A. G. Khachaturyan, G. Akcay, and Y. Ni, J. Appl. Phys. **103**, 114113 (2008).
[22]S. Zhukov, S. Fedosov, J. Glaum, T. Granzow, Y. A. Genenko, and H. von Seggern, J. Appl. Phys. **108**, 014105 (2010).
[23]J. Schütrumpf, S. Zhukov, Y. A. Genenko, and H. von Seggern, J. Phys. D: Appl. Phys. **45**, 165301 (2012).
[24]W. J. Merz, Phys. Rev. **95**, 690 (1954).
[25]W. Kleemann, Annu. Rev. Mater. Res. **37**, 415 (2007).
[26]E. Fatuzzo, Phys. Rev. **127**, 1999 (1962).
[27]M. Vopsaroiu, J. Blackburn, M. G. Cain, and P. M. Weaver, Phys. Rev. B **82**, 024109 (2010).
[28]M. Vopsaroiu, P. M. Weaver, M. G. Cain, M. J. Reece, and K. B. Chong, IEEE Trans. Ultrason. Ferroelectr. Freq. Control **58**, 1867 (2011).